COBEM 2023 27TH INTERNATIONAL CONGRESS OF MECHANICAL ENGENEERING

ABCM Brazilian Society of Mechanical Sciences and Engineering
27th ABCM International Congress of Mechanical Engineering
December 04-08, 2023, Florianópolis-SC, Brazil

COB-2023-0675
ONE-DIMENSIONAL NUMERICAL ANALYSIS OF A 5 KN LIQUID PROPELLANT ROCKET ENGINE COMBUSTION CHAMBER USING ETHANOL/LOX

Luiz Henrique Schaffazick
César Addis Valverde Salvador
Universidade Federal de Santa Maria
luiz.schaffazick@acad.ufsm.br
valverde@ufsm.br

Fernando S. Costa
Marcio T. Mendonca
Instituto Nacional de Pesquisas Espaciais
fernando.costa@inpe.br
marcio_tm@yahoo.com

Abstract. *Liquid bipropellant propulsion systems are widely used in launch rockets for their high thrust and specific impulse, increased operational and storage safety, and improved combustion control compared to solid propellant systems. In recent years, studies on green propulsion have become increasingly common due to the advantages it offers, such as lower pollutant emissions, low toxicity, reduced environmental impact, higher operational safety, lower propellant storage and handling costs, improved safety, and energy independence. Green propellants are cleaner and more sustainable compared to traditional chemical propellants. This work presents a numerical study of a 5 kN liquid rocket engine combustion chamber, which uses Ethanol and LOX as propellants. For the simulations, a one-dimensional, reactive, multiphase, and steady-state mathematical model of combustion in a combustion chamber was used. The model considers that the chemical reaction is faster than droplet vaporization, so that the propellant vapors mix and react instantaneously. The model also accounts for combustion at subcritical pressures, non-uniform fuel and oxidizer droplet size distributions, droplet preheating, heat losses from gas to chamber walls and droplets, different droplet and gas velocities, as well as the effect of deformation on droplet drag. Discrete portions of droplets with characteristic mean diameters are considered to represent the Rosin-Rammler distribution function, thus allowing the estimation of the vaporization length of a bipropellant spray under various conditions. The combustion products include 5 main species (CO_2, CO, H_2O, H_2, and O_2) and 3 secondary species (H, OH, and O). The obtained results allow evaluating the influence of pressure, propellant temperatures, equivalence ratio, number of propellant droplet portions, and Rosin-Rammler parameters on the complete vaporization distance. Theoretical values of vaporization distance and temperatures were determined and compared to data from the European project PERSEUS.*

Keywords: *Green Propellants, Modelling, Ethanol, Oxygen, Combustion Chamber*

1. INTRODUCTION

Rocket propulsion forms the fundamental basis of space exploration, sustaining the ambitious journey of human beings to comprehend the mysteries of the cosmos. Among the various propulsion mechanisms, liquid bipropellant systems are the most commonly used in launch rockets due to their high thrust generation, improved safety, and better combustion control compared to their solid propellant counterparts. Combustion chambers of liquid propellant rockets are essential components in converting propellant into high-pressure and high-temperature gases, generating thrust.

Liquid Propellant Rocket Engines (LPREs) can be classified into monopropellants, using a single propellant, or bipropellants, employing a propellant pair (fuel and oxidizer). The choice of the fuel-oxidizer pair and its mixture ratio is crucial to ensure sufficient energy is provided to achieve high exhaust velocity and obtain the necessary thrust, thus ensuring the success of a space mission.

In recent years, there has been a significant shift in propellant choices, with a growing preference for green propulsion (Gohardani et al., 2014). This change is driven by the advantages offered by green propellants, which include reduced pollutant emissions, low toxicity, lower environmental impact, improved operational safety, decreased storage and handling costs of propellants, and the potential for achieving energy independence. These benefits make green propellants a cleaner and more sustainable option compared to traditional chemical propellants. Among them, the combination of ethanol with liquid oxygen (Ethanol/LOX) has emerged as a promising alternative.

NASA has been using non-toxic and cryogenic propellant blends, such as LOX/Ethanol and LOX/LCH_4, in spacecraft reaction control systems (RCS), as they offer higher performance, ease of handling, and compatibility with propellants that can be produced in situ on the Moon or Mars (Cardiff et al., 2014; Klem et al., 2017).

Hurlbert et al. (2008) developed and tested a cryogenic RCS. Multiple system-level tests were conducted using multiple thrusters with cryogenic propellants in a simulated space environment. They conducted over 1600 tests with LOX/Ethanol and 733 tests with LOX/LCH_4. Their results highlighted the challenges encountered in managing cryogenic fluids and engine performance.

Gottmann et al. (2015) emphasized the importance of adopting green propellant pairs as substitutes for highly toxic hydrazines, highlighting Ethanol/LOX as a viable alternative due to its low toxicity and availability.

Sakaki et al. (2015) studied and tested thrust modulation in liquid rocket engines for various space missions, such as planetary descent, hazard avoidance, and orbital maneuvers. They observed the difficulty in maintaining combustion stability at low thrust levels due to inadequate atomization and mixing. In their findings, several solutions were proposed, including the incorporation of variable-area injectors and pintle injectors. The authors emphasized the need for further investigation into spray and flame structure using high-speed imaging techniques for an Ethanol/LOX combustor employing a pintle injector.

Sakaki et al. (2016) analyzed the influence of propellant injection systems on the performance of liquid propellant rocket engines, with a focus on the pintle type injector. They highlighted its simplicity, power control capability, and combustion stability. In their tests with pintle type injectors using Ethanol and LOX, they compared the performance of a rectangular combustor and an axi-symmetric combustor.

Delpy and Oswald (2017) conducted cold flow tests on the MLE5K-S1a engine that utilizes Ethanol/LOX as propellants. They obtained higher than expected discharge coefficient values of 6% for ethanol and 2% for liquid oxygen in cold flow conditions.

Da Silva Mota et al. (2018) developed a 7.5 kN (L75) Ethanol/LOX thruster at the Institute of Aeronautics and Space (IAE). The L75 engine was developed by IAE in partnership with the German Aerospace Center (DLR) for use in the third stage of the Brazilian Satellite Launch Vehicle, VLS-1. The objective was to replace the last two solid stages of the rocket with a single stage using Ethanol and LOX. Brazil does not yet have a complete cryogenic engine, although L5, L15, and L75 use LOX as the oxidizer (Gontijo et al., 2020).

Mayer et al. (2018) demonstrated that green fuels have a reduced environmental impact compared to traditional fossil fuels such as gasoline and diesel. The application and development of green propellants have increased in recent decades due to the pursuit of cost reduction, decreased storage and operational risks, environmental impact mitigation, and reduction of harm to human health. An increasing number of projects, such as the Green Advanced Space Propulsion (GRASP) (Scharlemann, 2011) and the Green Propellant Infusion Mission (GPIM) (McLean, 2013), are emerging, paving the way for further research related to green propulsion.

This work aims to analyze the behavior of an Ethanol/LOX spray in the combustion chamber of a 5 kN liquid rocket engine using a one-dimensional numerical model. The model was developed and validated by Salvador (2004) and considers a one-dimensional, steady, reactive, and multiphase flow in a combustion chamber. It assumes that chemical reactions occur more rapidly than droplet vaporization, so the combustion process is controlled by vaporization. The model also takes into account non-uniform distributions of fuel and oxidizer droplets at the chamber inlet, preheating of the droplets, convective and radiative heat losses from the gas to the chamber walls and droplets, different velocities of the droplets and gas, as well as the effect of droplet deformation on drag.

The main feature of this model is its ability to determine an appropriate number of droplet parcels to represent the Rosin-Rammler distribution functions used to describe the fuel and oxidizer spray droplet size distributions in the combustion chamber, thus allowing an estimation of the complete vaporization distance of a bipropellant spray under various conditions. The studied combustion products include eight species, five major species: CO_2, CO, H_2O, H_2, O_2, and three secondary species: H, OH, and O.

The results of this work provide important insights into the influence of pressure, temperature, equivalence ratio, droplet size distribution, convective and radiative heat losses, propellant vaporization rate, as well as Rosin-Rammler parameters on the complete evaporation distance. The model also considers variable thermodynamic properties, such as pressure- and temperature-dependent droplet vaporization enthalpies. This increases the accuracy of the model compared to other models, even at supercritical pressures.

The software was written in MATLAB 6.5 with a simple and versatile interface that can be used for any combination of liquid propellants with known thermodynamic and transport properties.

2. METHODOLOGY

2.1 Mathematical Model

Figure 1 depicts a schematic of the reactive process within a bipropellant combustion chamber. The model considers the injection of spherical droplet sprays through an injector plate into the combustion chamber, containing multiple droplet parcels. Each parcel includes droplets within a known diameter range entering the combustion chamber. It is assumed

that all diameter ranges have equal width. For example, a cloud of sprays with droplet diameters ranging from 0 to 140 μm can be represented by 4 ranges or parcels as follows: 0-35, 35-70, 70-105, 105-140 μm.

To simplify the analysis, each parcel is characterized by a representative mean diameter (SMD). The procedure to obtain the representative SMD of a droplet parcel is described in Salvador (2004). The size distribution of fuel and oxidizer droplets in the spray is described by Rosin-Rammler distribution functions, whose parameters can be obtained experimentally and vary with the type of injector. A maximum droplet diameter, D_{max}, is calculated for the different Rosin-Rammler distributions of the fuel and oxidizer, above which the volume percentage of propellant is less than 0.1%. In other words, droplets with a diameter larger than D_{max} are not considered.

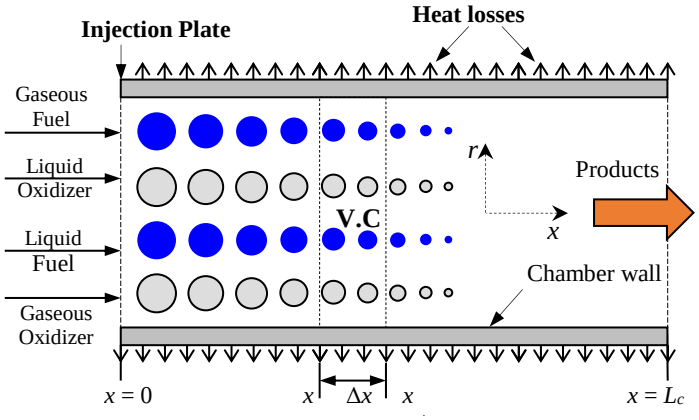

Figure 1. One-dimensional model of a bipropellant combustion chamber.

In a simplified term, the operation takes place by injecting the propellants into the chamber in the form of liquid jets, which immediately transform into sprays containing small droplets that are heated by the hot gas in the chamber, expand, and vaporize as they are transported by the flow. The fuel and oxidizer vapors mix and burn, resulting in the formation of new products that change the local composition. This process continues until all the mass of the liquid propellants is converted into products. The pressure is assumed to be uniform, but the gas temperature varies along the chamber due to changes in the equivalence ratio of the mixture. Initially, the gases and droplets have different velocities, but as the droplets vaporize, the gas-droplet relative velocity tends to zero.

It is assumed that 10% of the total fuel and oxidizer are injected in the form of gases to create a gas flow near the injection plate, corresponding to recirculating flows in real systems. Several factors, such as gas recirculation, high gas velocities, injection configuration, chamber geometry, liquid jet impact, and flow with different phase velocities, generate intense turbulent mixing, making droplet vaporization rates a controlling factor. The model also considers transient vaporization, following the methodology presented by Lefebvre and McDonell (2017).

Since turbulent mixing and combustion are fast compared to vaporization, the gas composition is calculated in each section assuming pressure and temperature equilibrium, but considering heat transfer through convection and radiation from the gas mixture to the chamber walls and droplets. Heat losses through conduction to the environment, through the chamber wall, are also considered.

Droplet vaporization during the transient phase can be significant and depends on the thermodynamic properties of the gas mixture. Borman and Ragland (1998) showed that significant vaporization occurs during droplet preheating. The thermal expansion of the droplet is considered during the heating phase until the droplet reaches an equilibrium temperature or wet-bulb temperature, at which point the droplet diameter begins to continuously decrease.

2.2 Rosin-Rammler Distribution Function

There are several empirical relationships to characterize the droplet size distribution in a cloud of droplets or spray. The Rosin-Rammler distribution function is the most commonly used due to its simplicity (Lefebvre, 1989), with only two parameters to be determined, q and D_{32}. It allows extrapolation of experimental data to very small droplet diameters that are difficult to measure. The Rosin-Rammler function is expressed in terms of the cumulative volume fraction, Q:

$$Q = 1 - \exp\left[-\Gamma\left(1 - 1/q\right)^{-q} \left(D/D_{32}\right)^{q} \right] \tag{1}$$

where Q is the volume fraction of the spray containing droplets with diameters smaller than D, and q and D_{32} are constants. The parameter q measures the uniformity of the spray, where an increase in q results in a more uniform spray, and if q is infinite, then all droplets have the same diameter. According to Lefebvre, in most sprays, q ranges between 1.5 and 4. On the other hand, the parameter D_{32} represents the Sauter Mean Diameter (SMD), and Γ is the gamma function.

Figure 2 shows the influence of the number of droplet parcels on the Rosin-Rammler distribution, with D_{32} = 30 µm and q = 2, using Ethanol and LOX, for N = 4 and 12 parcels. Salvador (2004) found that a higher number of parcels, representing the diameter distribution, leads to more accurate results as there is a better distribution of analyzed droplet diameters. However, it should be considered that an increase in the number of parcels also increases the computation time.

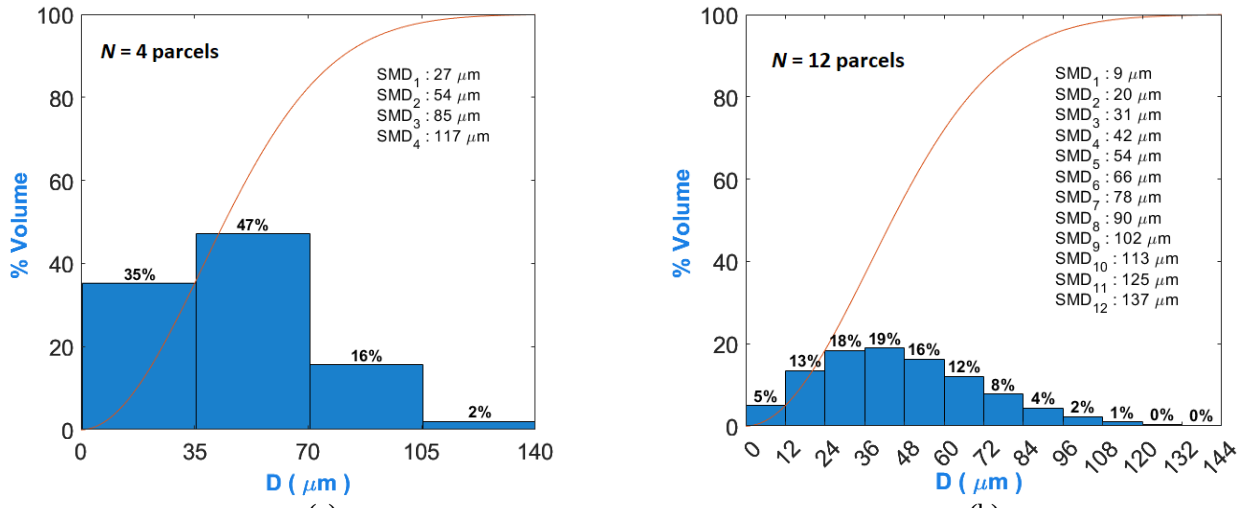

(a) (b)

Figure 2. Rosin-Rammler distribution function for D_{32} = 30 µm and q = 2 (a) N = 4 parcels; (b) N = 12 parcels.

In Figure 2.a, for example, the droplet size distribution is shown for a total of 4 parcels. It can be observed that 47% of the total spray volume is composed of droplets with diameters ranging from 35-70 µm. For the parcel with the smallest volume, around 2%, the droplets are distributed between 105-140 µm. In this case, since 4 parcels of equal volume were considered, the representative diameters for each volume are, respectively: 27, 54, 85, and 117 µm. In other words, the 27 µm droplet represents all the droplets ranging from 1 to 35 µm, and so on for the other parcels.

In Figure 2.b, which represents the case of 12 parcels of droplets distributed in the spray, it can be concluded that a higher number of parcels leads to greater accuracy in the droplet size distribution and a smoother curve compared to, for instance, a distribution with 4 parcels. It can be noted that the two largest volumes, 18% and 19%, are represented by droplets between 24-36 µm and 37-48 µm, respectively. It is also observed that droplets above 108 µm have a volume of less than 2% and can often be disregarded in numerical calculations. Salvador (2004) showed in their results that considering more than 12 parcels already provided reasonably accurate results.

2.3 Conservation Equations

Mass and energy balances in control volumes provide a system of ordinary differential equations that can be numerically integrated, given the initial conditions. The mass balance is given by,

$$\frac{d\dot{m}_g}{dx} + \frac{d\dot{m}_{F,l}}{dx} + \frac{d\dot{m}_{Ox,l}}{dx} = 0 \tag{2}$$

where the subscripts "F" and "Ox" designate the fuel and oxidizer, respectively, and the subscripts "g" and "l" designate the phases present in the chamber, gas and liquid, respectively. Therefore, m_g, $m_{F,l}$, and $m_{Ox,l}$ are the mass flow rates of the gas, fuel, and liquid oxidizer, respectively.

The energy balance equation results,

$$\frac{dT_g}{dx} = -\left(a_1 + W_F + W_{Ox} + \frac{d\dot{Q}_{conv,p}}{dx} + \frac{d\dot{Q}_{rad,p}}{dx} \right) \Big/ a_2 \tag{3}$$

where T_g is the temperature of the gases in the chamber, $\dot{Q}_{conv,p}$ and $\dot{Q}_{rad,p}$ are the convective and radiative heats transferred from the gas to the walls and droplets, a_1 and a_2 are functions of the gas mixture, and W_F and W_{Ox} are functions of the liquid phase, fuel and oxidizer, respectively, given by,

$$a_1 = \dot{m}_g v_g^2 \left[\frac{3}{2\dot{m}_g} \frac{d\dot{m}_g}{dx} - \frac{1}{A_g} \frac{dA_g}{dx} \right] + \left[\dot{m}_g \frac{dh_g}{d\Phi} \frac{d\Phi}{dx} + h_g \frac{d\dot{m}_g}{dx} \right] \tag{4}$$

$$a_2 = \dot{m}_g \left[\frac{dh_g}{dT_g} - v_g^2 \left(\frac{1}{\bar{M}_g} \frac{d\bar{M}_g}{dT_g} - \frac{1}{T_g} \right) \right] \tag{5}$$

$$\mathrm{W_F} = \sum_{i=1}^{I} \dot{m}_{F,l,i} C_{pF,l,i} \frac{dT_{F,l,i}}{dx} + h_{F,l,i} \frac{d\dot{m}_{F,l,i}}{dx} + \sum_{i=1}^{I} \dot{m}_{F,l,i} v_{d,F,i} \frac{dv_{d,F,i}}{dx} + \frac{v_{d,F,i}^2}{2} \frac{d\dot{m}_{F,l,i}}{dx} \tag{6}$$

$$\mathrm{W_{Ox}} = \sum_{j=1}^{J} \dot{m}_{Ox,l,j} C_{pOx,l,j} \frac{dT_{Ox,l,j}}{dx} + h_{Ox,l,j} \frac{d\dot{m}_{Ox,l,j}}{dx} + \sum_{j=1}^{J} \dot{m}_{Ox,l,j} v_{d,Ox,j} \frac{dv_{d,Ox,j}}{dx} + \frac{v_{d,Ox,j}^2}{2} \frac{d\dot{m}_{Ox,l,j}}{dx} \tag{7}$$

$$\frac{d\dot{Q}_{conv,p}}{dx} = \hat{h}_g \pi D_c \left(T_g - T_{wi} \right) \tag{8}$$

$$\frac{d\dot{Q}_{rad,p}}{dx} = \varepsilon_g \sigma \pi D_c \left(T_g^4 - T_{wi}^4 \right) \tag{9}$$

where v_g, A_g, h_g, M_g, $\hat{h}_g$ and ε_g are velocity, area, enthalpy, molar mass, convective coefficient, and gas emissivity, respectively, and Φ is the equivalence ratio. For the liquid phase, C_{pl}, T_l, and h_l are the specific heat at constant pressure, temperature, and enthalpy of the liquid, respectively, and v_d, D_c, T_{wi} and σ are the droplet velocity, chamber diameter, internal chamber wall temperature, and Stefan-Boltzmann constant, respectively.

The system of nonlinear equations is numerically integrated using MATLAB program routines. Details of the numerical and computational techniques employed are provided in Salvador (2004).

2.4 PERSEUS Project - L5

The PERSEUS project emerged as an incentive for European students to apply the knowledge acquired in the field of nano-satellite launch rocketry. Within the PERSEUS project, there is the Minerva project, which aims to develop and test bipropellant engines. The first propulsion system developed by the Minerva project (Delpy and Oswald, 2017) was the MLE5K-S1a, which uses Ethanol and LOX as propellants and has a thrust of 5 kN. In this work, the input parameters will consider the data of the MLE5K-S1a propulsion system. Its combustion chamber has a diameter of 12 cm and a length of 35 cm, and the throat diameter of the nozzle is 4.95 cm. A simplified diagram of the combustion chamber is shown in Figure 3.

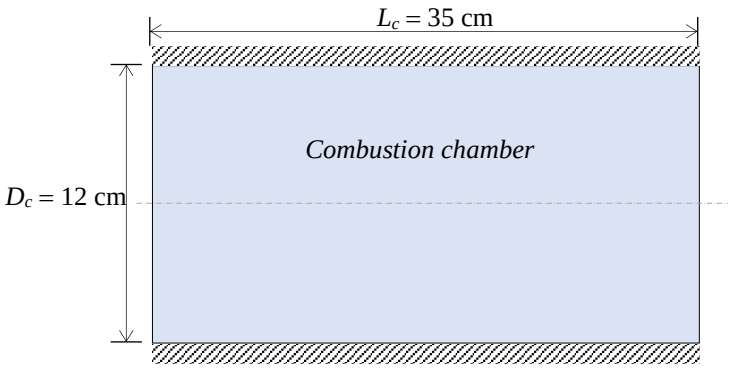

Figure 3. Simplified diagram of the combustion chamber of the MLE5K-S1a.

Furthermore, the inlet temperatures of the fuel and oxidizer were considered $T_{F,o}$ = 300 K and $T_{Ox,o}$ = 90 K, respectively. Among other data, 12 droplet parcels were adopted for each of the propellants, and the Rosin-Rammler parameters D_{32} = 30 μm and q = 2 were used for both the fuel and oxidizer. The remaining characteristics of this thruster are described in Table 1.

Table 1. MLE5K-S1a Thruster Features (Delpy and Oswald, 2017).

Properties	
Max thrust in vacuum	5 kN
Thrust at sea level	4.3 kN
LOX mass flow	1.15 kg/s
Ethanol mass flow	0.81 kg/s
Total mass flow	2.04 kg/s
Combustion temperature	3100 K
Combustion efficiency	0.95
Chamber pressure	20 bars
Combustion time	20 s
I_{sp} at sea level	260 s
I_{sp} in vacuum	295 s
Mixing ratio, O/F	1.42
LOX injection velocity	27 m/s
Ethanol injection velocity	33 m/s

2.5 Combustion Products

The model developed by Salvador (2004) allows for the identification of up to 11 species as combustion products, including 6 main species with high concentration: CO_2, CO, H_2O, H_2, O_2, and N_2, and 5 secondary species with low concentration: H, OH, O, NO, and N. Other secondary species could have been considered, such as HO_2, H_2O_2, etc., but their concentration is found to be very low compared to the 11 species considered.

In this work, only 8 species were adopted as combustion products, including 5 main species: CO_2, CO, H_2O, H_2, O_2, and 3 secondary species: H, OH, and O, because the reactants do not include nitrogen-based compounds.

3. RESULTS

3.1. Vaporization Length

In the design of the combustor, the distance at which complete vaporization of the propellants occurs is considered one of the most important parameters as it directly influences combustion efficiency. Oversized chambers can increase project costs because if more material is used in manufacturing, the chamber's weight, and consequently, the spacecraft's weight, will be greater, reducing the efficiency of the propulsion system. Conversely, in chambers with dimensions smaller than ideal, propellant droplets may not vaporize and burn completely during their passage through the chamber, resulting in unburned liquid reactants passing through the nozzle, leading to low engine performance.

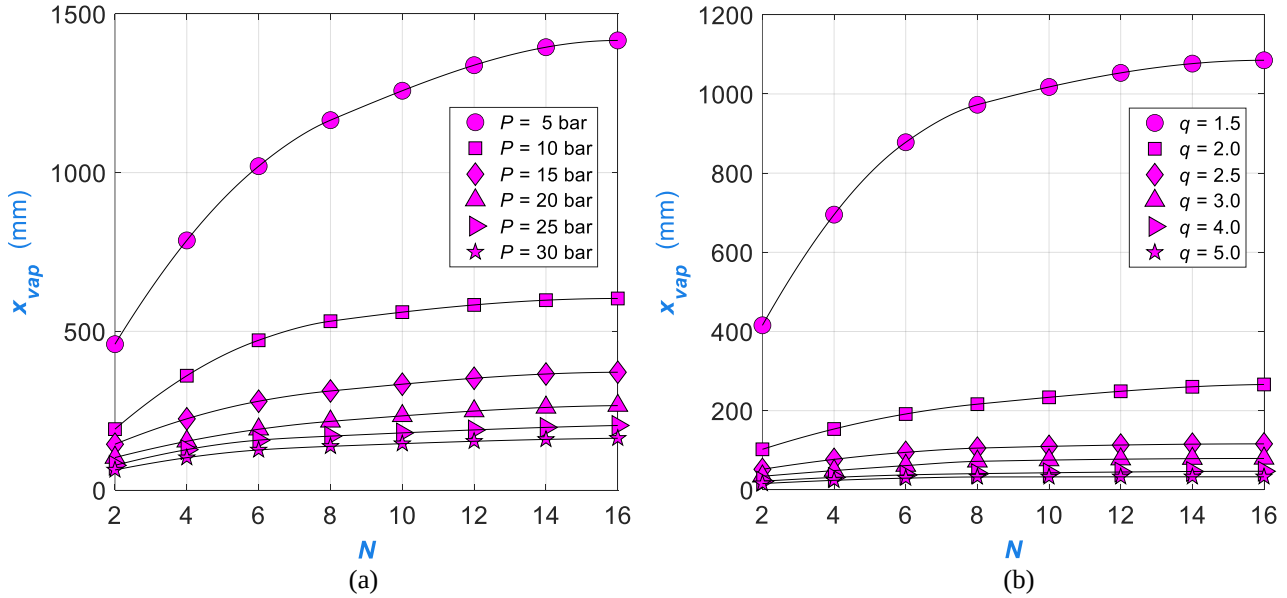

(a) (b)

Figure 4. Influence of the number of droplet parcels, N, entering the combustion chamber on the vaporization length, x_{vap}, for Ethanol. $T_{g,0}$ = 600 K, $T_{F,l,0}$ = 300 K, $T_{Ox,l,0}$ = 90 K, Φ_T = 1,467, D_{32} = 30 μm. (a) q = 2, (b) P = 20 bar.

The Rosin-Rammler parameters D_{32} = 30 μm and q = 2 were used to obtain Figures 4.a and 5.a. The gas mass flow rates of fuel and oxidizer at the inlet were considered to be 10% of the liquid mass flow rates. The injected gas mass fractions at the inlet correspond to recirculating flows in real systems.

The Figure 4.a depicts the influence of the number of droplet parcels, N, admitted at the chamber inlet, on the complete vaporization distance of Ethanol droplets, x_{vap}, for pressures ranging from 5 to 30 bar. It is observed that as the number of parcels increases, the curves exhibit a tendency toward convergence. It is also concluded that for pressures above 15 bar, a total of 8 droplet parcels may suffice to generate results with adequate accuracy for x_{vap}. Furthermore, it is observed that for pressures below 15 bar, the appropriate number of parcels should be greater than 12. For pressures greater than 25 bar, the choice of 6 droplet parcels may be sufficient to ensure a good estimate of the vaporization length.

On the other hand, Figure 4.b presents the influence of the number of Ethanol droplet parcels, N, on x_{vap}, for variations of the Rosin-Rammler parameter, q, ranging from 1.5 to 5. The parameter q measures the spray uniformity, where an increase in q leads to a more uniform spray, such that if q is infinite, all droplets have the same diameter. According to Lefebvre, in most sprays, the value of q ranges between 1.5 and 4. It is noticed that, the smaller the value of q, the greater the vaporization length, because as q decreases, the probability of encountering larger droplet diameters increases, which take longer to vaporize and burn completely. Salvador and Costa (2006) demonstrated in their results that the maximum droplet diameter, D_{max}, in a spray, using the Rosin-Rammler distribution function, increases as the value of q decreases. Figure 6 shows how the increase in q results in a decrease in the maximum droplet diameter, D_{max}. For q = 1.5, D_{max} was 260 μm, and for q = 2, the maximum diameter found was 124 μm.

Figure 5.a illustrates the influence of the chamber's internal pressure, P, on the vaporization length of Ethanol, x_{vap}. From the graph, it can be observed that as P increases, x_{vap} decreases, since an increase in pressure causes an increase in the liquid vaporization rate (Chin and Lefebvre, 1983). The graphs include results for 3 droplet size distributions or number of parcels, N, i.e., for 1, 2, and 3 droplet parcels. The choice of an appropriate number of parcels is important because using a large number of parcels can excessively increase the calculation time, while a small number of parcels may produce large errors in the estimation of the vaporization length.

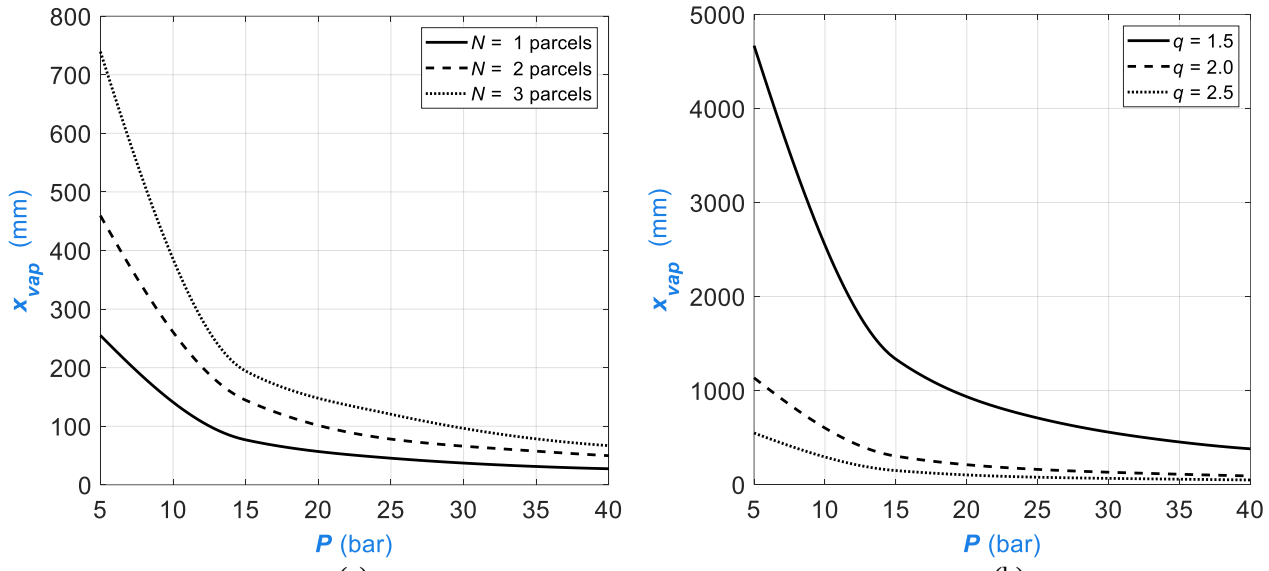

(a) (b)

Figure 5. Influence of the internal pressure of the combustion chamber, P, on the vaporization length, x_{vap}, for Ethanol, $T_{g,0}$ = 600 K, $T_{F,l,0}$ = 300 K, $T_{Ox,l,0}$ = 90 K, Φ_T = 1,467, D_{32} = 30 μm. (a) q = 2, (b) N = 8 parcels.

Figure 5.b shows the variation of Ethanol's x_{vap} with pressure, P, while varying the Rosin-Rammler parameter, q. It can be observed that for q = 2.5 and pressures above 15 bar, the vaporization length does not vary significantly, with D_{32} = 30 μm and N = 8 parcels. Salvador and Costa (2006) demonstrated in their results that for Hidrazine/N_2O_4 mixtures, using q values above 2 already yielded adequate results for x_{vap}. It is also noted that for q = 1.5, the vaporization length increases sharply, as the D_{max} of the droplet in the spray increases as q decreases.

Figures 6.a and 6.b present the variation of the dimensionless droplet diameter, D/D_0, along the combustion chamber for 6 droplet parcels, P = 20 bar, and D_{32} = 30 μm, for both fuel and oxidizer, for q values of 1.5 and 2, respectively. It can be seen that for q = 1.5, the spray contains droplets with larger representative diameters, SMD = 36, 75, 120, 166, 213, and 260 μm, compared to a spray using q = 2, with SMD = 18, 37, 58, 80, 102, and 124 μm. In Figure 6.a, fuel droplets with D_{max} = 260 μm completely vaporize at a distance of 880 mm from the chamber inlet, while for oxidizer droplets of the same diameter, complete vaporization occurs at a distance of 455 mm. In the case of Figure 6.b, fuel droplets with D_{max} = 124 μm vaporize at a distance of 193 mm, and oxidizer droplets of the same diameter vaporize at 138 mm. In both results, it can be observed that the larger the droplet diameter, the longer the combustion chamber should

be to ensure complete vaporization within it. It is also evident that the fuel vaporizes and burns faster than the oxidizer when using the same droplet diameters and number of parcels, this is because LOX has a higher vaporization rate than Ethanol, as shown in Figure 7.

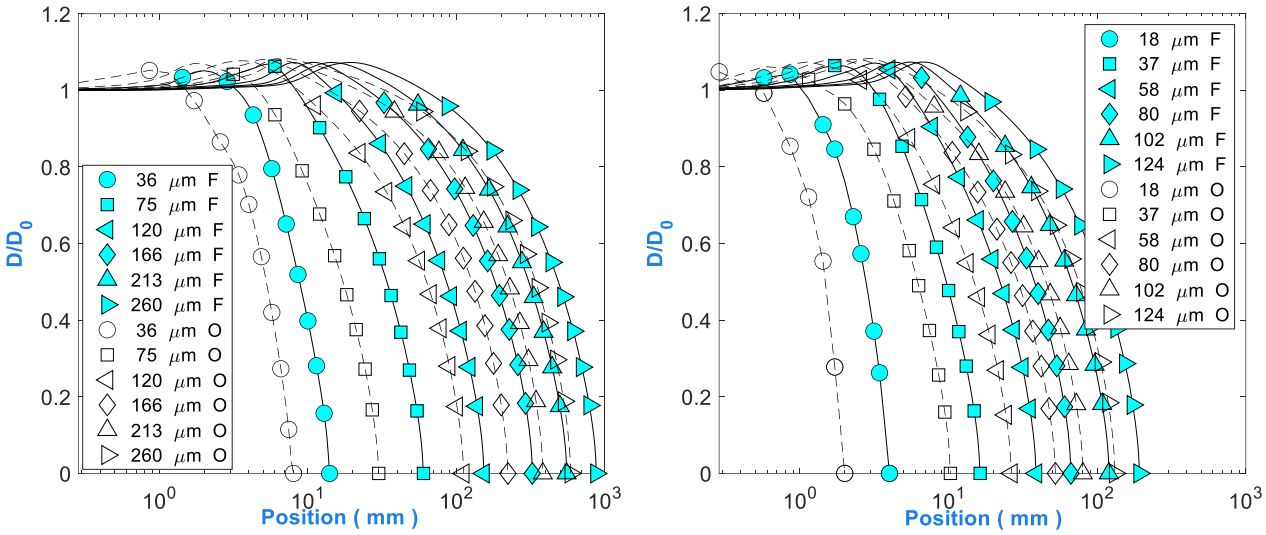

(a) (b)

Figure 6. Variation of the dimensionless droplet diameter: N = 6 parcels, P = 20 bar e D_{32} = 30 μm (a) q = 1,5; (b) q = 2

Figures 7.a and 7.b show the variation of the vaporization rate as a function of distance for droplets of various representative diameters of fuel and oxidizer, in kg/s. The vaporization rate increases during the droplet preheating period until the droplet reaches its equilibrium temperature at the chamber pressure, and then decreases until complete evaporation of the droplets. The vaporization rate is directly proportional to the droplet diameter and increases due to its expansion.

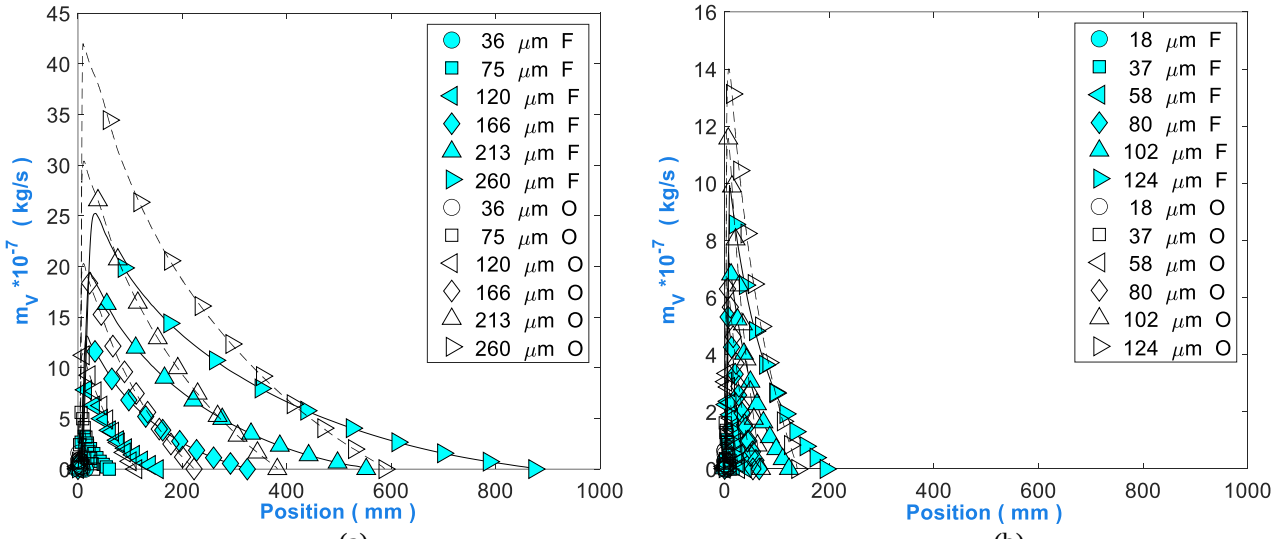

(a) (b)

Figure 7. Variation of the vaporization rate of fuel and oxidizer droplets: N = 6 parcels, P = 20 bar e D_{32} = 30 μm (a) q = 1,5; (b) q = 2.

3.2. The MLE5K-S1a engine

In Figure 8.a, the variation of the dimensionless droplet diameter, D/D_0, along the combustion chamber proposed by Delpy and Oswald (2017), with a length of L_c = 35 cm, is shown. Twelve droplet parcels were used, with Rosin-Rammler parameters of q = 2 and D_{32} = 30 μm, for both fuel and oxidizer. All data for this engine (MLE5K-S1a) are presented in Table 1. It can be observed that the maximum droplet diameter under these conditions was 137 μm, for both fuel and oxidizer. Fuel droplets take more time to vaporize than oxidizer droplets of the same diameter. In practice, the vaporization rate of LOX is higher than that of Ethanol, according to Sieder et al. (2017). To allow the oxidizer droplets to completely vaporize at the same distance as the fuel droplets, a larger D_{32} could be adopted for the oxidizer, for example, 50 μm

instead of 30 μm, as larger droplets take more time to vaporize. In practice, this would be equivalent to constructing a LOX injector plate with larger exit channels, compared to the Ethanol injector plate, as described by Schaffazick and Salvador (2023). In the detail of the expansion region, it can be observed that the dimensionless droplet diameter increases by about 6% to 8%, for both propellants, until reaching the wet bulb temperature, and then continuously decreases in size until complete vaporization.

In Figure 8.b, temperature and equivalence ratio profiles of the gases in the chamber (combustion products) are shown. The gas temperature increases from 600 K at the inlet until reaching the maximum temperature of 3370 K at 12 mm from the chamber inlet, when the equivalence ratio is approximately $\Phi = 1.3$. In most small propellants without regenerative cooling, a protective curtain or layer of liquid propellant is used near the wall to reduce the wall temperature and prevent it from exceeding the temperature limits that cause material failure. The stoichiometric O/F mixture ratio for the bipropellant pair, Ethanol/LOX, is $f_s = 2.084$; however, the engine proposed by Delpy and Oswald (2017) operates at $f_x = 1.42$, resulting in a calculated equivalence ratio of $\Phi = 1.467$, meaning the engine operates with excess fuel, resulting in a high equivalence ratio throughout the combustion process. It is also noted that the equivalence ratio decreases to $\Phi = 0.95$ at 2 mm from the chamber inlet, as the O/C mixture ratio increases due to a greater increase in oxidizer vapor compared to Ethanol vapor. Subsequently, Φ gradually increases until reaching a maximum value of $\Phi = 1.4$ at 25 mm from the chamber inlet.

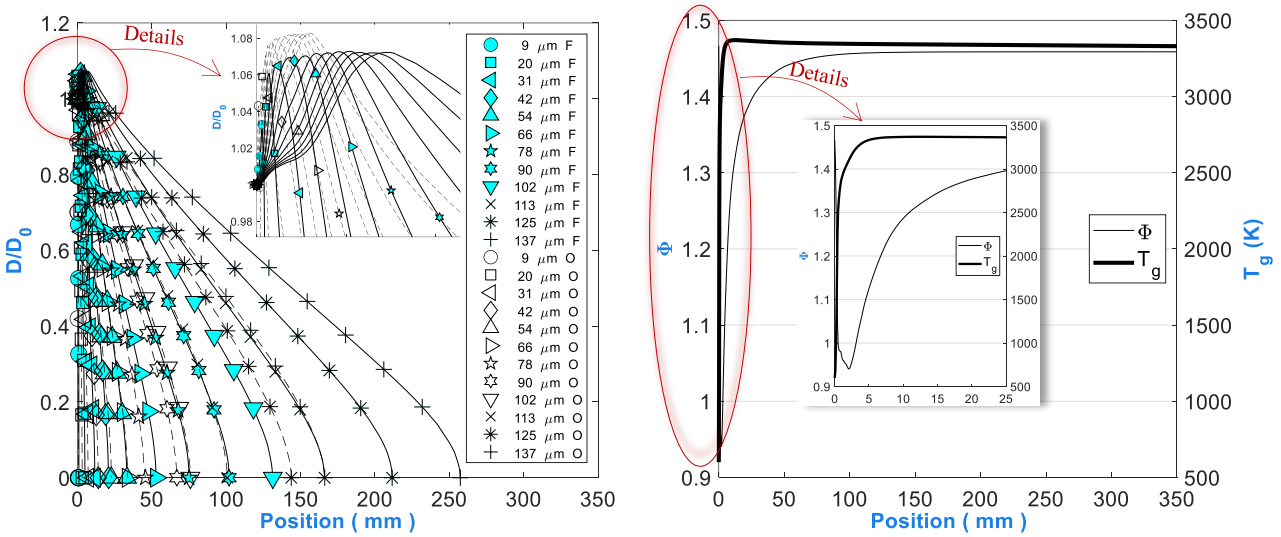

(a) (b)

Figure 8. Motor MLE5K-S1a: $N = 12$ parcels, $P = 20$ bar, $D_{32} = 30$ μm, $q = 2$. (a) Variation of the dimensionless droplet diameter showing details of the expansion region; (b) Evolution of the equivalence ratio and gas temperature in the chamber, showing details of the points of maximum temperature and minimum equivalence ratio.

4. CONCLUSIONS

This work presented a numerical study of the combustion chamber of the 5 kN engine developed by Delpy and Oswald (2017). The simulated rocket engine (MLE5K-S1a) uses Ethanol and LOX as propellants. The results shown were obtained using the one-dimensional mathematical model developed by Salvador (2004). The Rosin-Rammler function was used to describe the droplet size distribution in the combustion chamber of this engine, considering a total of 12 droplet parcels at the inlet for both fuel and oxidizer. It was found that complete vaporization of the droplets occurs approximately 25 cm from the chamber inlet, within the designed chamber length, which was 35 cm. The dimensionless droplet diameter, equivalence ratio, and gas temperature were presented and analyzed.

It was found that the size of the droplet expansion region depends not only on pressure but also on the initial temperature. This is because the closer the liquid inlet temperature is to the critical temperature, the shorter the heating period. Furthermore, it was observed that spray combustion models should include the preheating period due to the significant amount of mass vaporized during this phase.

The study found that the vaporization rate of LOX is higher than that of Ethanol for droplets of the same diameter, increasing as the Rosin-Rammler parameter q decreases.

The influence of the number of droplet parcels, N, on the complete vaporization length of Ethanol, x_{vap}, was analyzed for various pressures, P, and different values of the Rosin-Rammler parameter q. It was concluded that the higher the number of parcels, N, the more convergent the results of x_{vap} become, regardless of the pressure or the value of q. The influence of pressure on x_{vap} was also analyzed by varying N and q, and it was found that with increasing pressure, the vaporization length becomes more convergent for different values of N or q.

It was also observed that choosing an appropriate number of droplet parcels is important in calculating the complete vaporization distance and/or residence time of the droplets, thus estimating the length of the combustion chamber.

5. ACKNOWLEDGEMENTS

The authors would like to thank the Department of Mechanical Engineering (DEM) and the Aerospace Engineering Program at the Federal University of Santa Maria (UFSM) for the financial support to the first author.

6. REFERENCES

Borman, G. L.; Ragland, K. W., 1998. Combustion engineering. *New York: McGraw-Hill, 613p*.

Cardiff, E. H., Mulkey, H. W., & Baca, C. E., 2014. "An Analysis of Green Propulsion Applied to NASA Missions". *NASA Report, No. GSFC-E-DAA-TN14280.*

Chin, J. S.; Lefebvre, A. H. 1985. Steady-State Evaporation Characteristics of Hydrocarbon Fuel Drops. *AIAA Journal, v. 21, n. 10, p.1437-1443.*

Costa, E. M. S., Costa, F. S., Mendonça, M. T. 2022. "Simulação Numérica da Combustão de Sprays de Etanol e LOX" *Masters dissertation on Space Engineering and Technology/Combustion and Propulsion - INPE.*

Delpy R., Oswald, J. "Perseus Project 5kN LOX/Ethanol Rocket Engine Fire Tests". 2017. *7th European Conference for Aeronautics and Space Sciences (EUCASS)*.

Gohardani, A. S., Stanojev, J., Demairé, A., Anflo, K., Persson, M., Wingborg, N., & Nilsson, C., 2014. "Green space propulsion: Opportunities and prospects". *Progress in Aerospace Sciences, 71, 128-149.*

Gontijo, M.S., Fischer, G.A.A. and Costa, F.S., 2020. "Evaluation of smd effects on characteristic lengths of liquid rocket engines using ethanol/lox and rp-1/lox". 18th Brazilian Congress of Thermal Sciences and Engineering.

Gottmann, C. A., Alves, W. F., Rocco, J. A. F. F., Iha, K. & Gonçalves, R. F. B., 2015. "Liquid rocket propellants: Ethanol as fuel". *Global Journal of Advanced Research.*

Hurlbert, E., Villemarette, M., Angstadt, T., Collins, J., Peters, T., Allred, J., & Mahoney, J., 2008. "870lbf Reaction Control System Tests using LOx/Ethanol and LOx/Methane at White Sands Test Facility". *In 44th AIAA/ASME/SAE/ASEE Joint Propulsion Conference & Exhibit, p. 5247.*

Klem, M. D., 2017. "LOX/Methane In-Space Propulsion Systems Technology Status and Gaps". *In Southwest Emerging Technology Symposium (SETS) 2017, No. GRC-E-DAA-TN40702.*

Lefebvre, A. H., 1989. Atomization and sprays combustion. *New York: Hemisphere Publishing*.

Lefebvre, A.H. and McDonell, V.G., 2017. *Atomization and sprays*. CRC press.

Mayer, A., & Wieling, W., 2018. "Green propulsion research at TNO the Netherlands". *Transactions on aerospace research, 2018(4), 1-24.*

McLean, C. H., 2013. "Green propellant infusion mission program overview". *In 49th AIAA/ASME/SAE/ASEE Joint Propulsion Conference, p. 3847.*

Mota, F. A. D. S., Hinckel, J. N., Rocco, E. M., & Schlingloff, H., 2018. "Modeling and analysis of a LOX/Ethanol liquid rocket engine". *Journal of Aerospace Technology and Management, 10.*

Sakaki, K., Kakudo, H., Nakaya, S., Tsue, M., Isochi, H., Suzuki, K., & Hiraiwa, T., 2015. "Optical measurements of ethanol/liquid oxygen rocket engine combustor with planar pintle Injector". *In 51st AIAA/SAE/ASEE Joint Propulsion Conference, p. 3845.*

Sakaki, K., Kakudo, H., Nakaya, S., Tsue, M., Suzuki, K., Kanai, R., Hiraiwa, T., 2017. "Combustion characteristics of ethanol/liquid-oxygen rocket-engine combustor with planar pintle injector". *Journal of Propulsion and Power*, *33*(2), 514-521.

Salvador, C.A.V., 2004. "Modelo matemático de câmaras de combustão bipropelentes". *Masters dissertation on Space Engineering and Technology/Combustion and Propulsion - INPE.*

Salvador, C.A.V. and Costa, F.S., 2006. "Vaporization lengths of hydrazine fuels burning with NTO". *Journal of Propulsion and Power*, Vol. 22, No. 6, pp. 1362–1372.

Schaffazick L.H.; Salvador C.A.V. 2023. "Estudo numérico de uma câmara de combustão de motor foguete de 500N utilizando Etanol e LOX". *XXIX Congresso Nacional de Estudantes de Engenharia Mecânica*.

Scharlemann, C., 2011. "Green Advanced Space Propulsion-A project status". *In 47th AIAA/ASME/SAE/ASEE Joint Propulsion Conference & Exhibit, p. 5630.*

Sieder, J., Kleebusch, K., Bach, C. and Tajmar, M., 2017. "Development history and verification of the flight model of a 500 N Ethanol/LOX Rocket Engine". *7th European conference for aeronautics and aerospace sciences (EUCASS)*

7. RESPONSIBILITY NOTICE

The author(s) is (are) the only responsible for the printed material included in this paper.